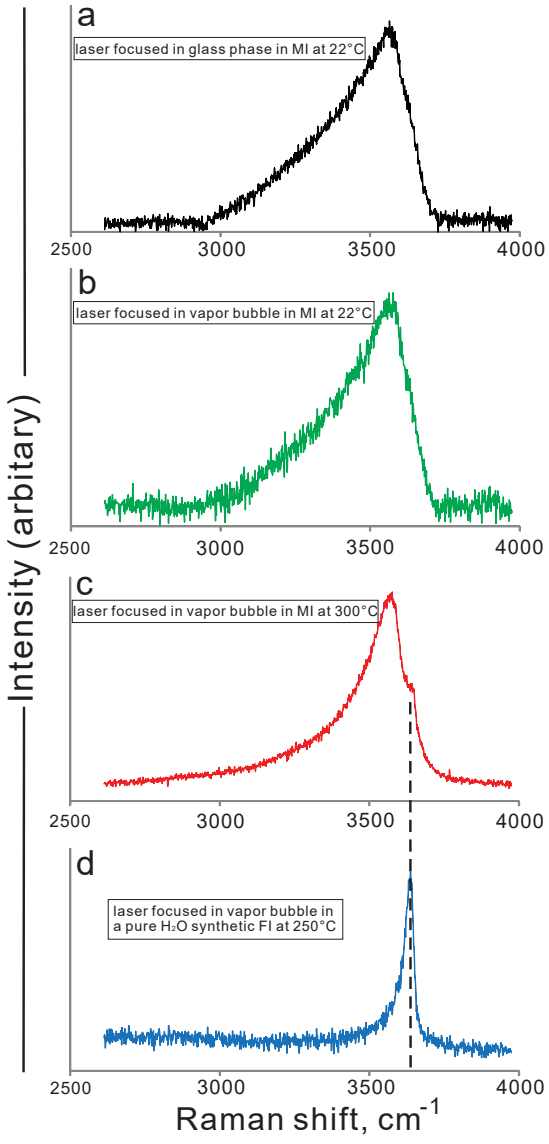

Figure OM1. Raman spectra collected from the glass and the vapor bubbles in MI and FI. (**a**) Raman spectrum collected at room temperature of the glass phase in a re-homogenized MI. The broad band corresponds to H_2O dissolved in the glass (melt) phase; (**b**) Raman spectrum obtained with the laser is focused on the vapor bubble in a re-homogenized MI at room temperature. The signal from the vapor bubble is masked by the signal from the surrounding glass phase; (**c**) Raman spectrum collected at 300°C from the vapor bubble in a re-homogenized MI; (**d**) Raman spectrum collected from the vapor phase in a synthetic pure water FI at 250°C. The position of the Raman peak for H_2O vapor shown in **d** suggests that the small shoulder on the broad band shown in **c** represents H_2O vapor in the bubble in this MI. The dashed line shows that the position of the Raman peak for H_2O vapor obtained from the synthetic fluid inclusion is at the same wavenumber as the small shoulder obtained from analysis of the vapor bubble in the MI.

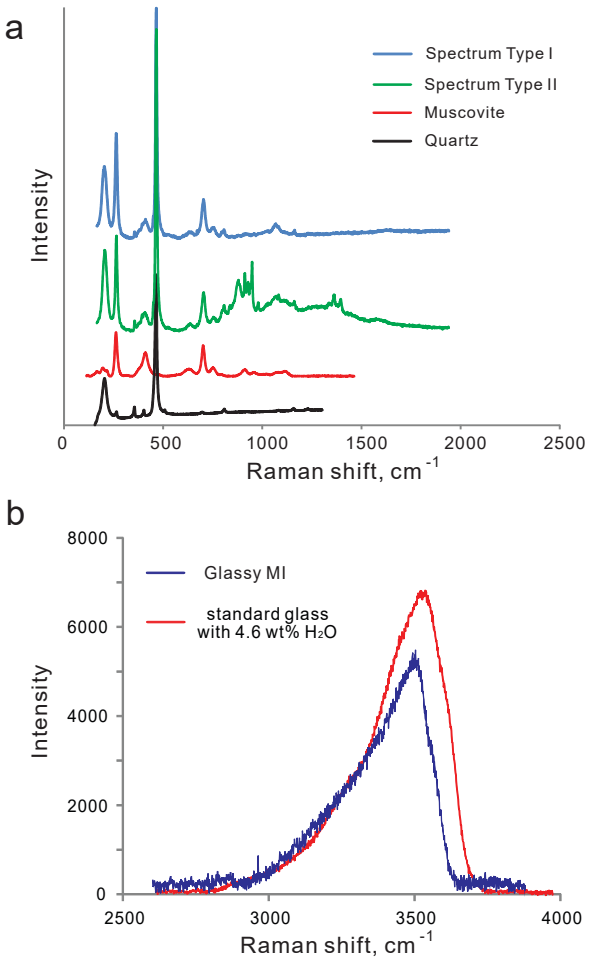

Figure OM2. (**a**) Raman spectra collected from unheated melt inclusions. Most show a mixture of muscovite and quartz, defined as Spectrum Type I; other spectra show a mixture of muscovite and quartz, as well as a complex band in the range 1000–800 cm^{-1}; (**b**) the Raman spectrum of H_2O in the glass phase of a re-homogenized melt inclusion in quartz. Also shown is the spectrum obtained from a glass standard containing 4.6 wt% H_2O.

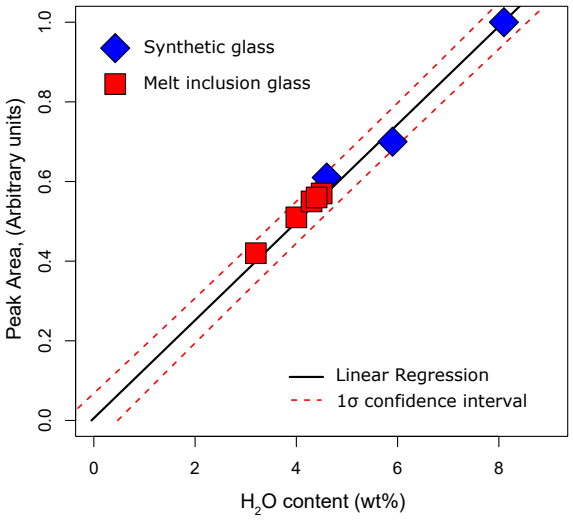

FIGURE OM3. The measured area under the H_2O Raman band vs. the H_2O content of the glass for MI (red squares) and standard glasses containing 4.6, 5.9, and 8.1 wt% H_2O (blue diamonds). The black solid line represents the calibration line derived from the relationship between the Raman band area and the H_2O content of the three standard glasses and the 1-sigma error is shown by the dashed lines. Severs et al. (2007) reported an uncertainty of ±0.1 wt% for H_2O analysis of glass using a technique similar to that used here, but we report a more conservative error of ~±0.4 wt% (1σ), which is approximately the size of the data symbols in the figure.

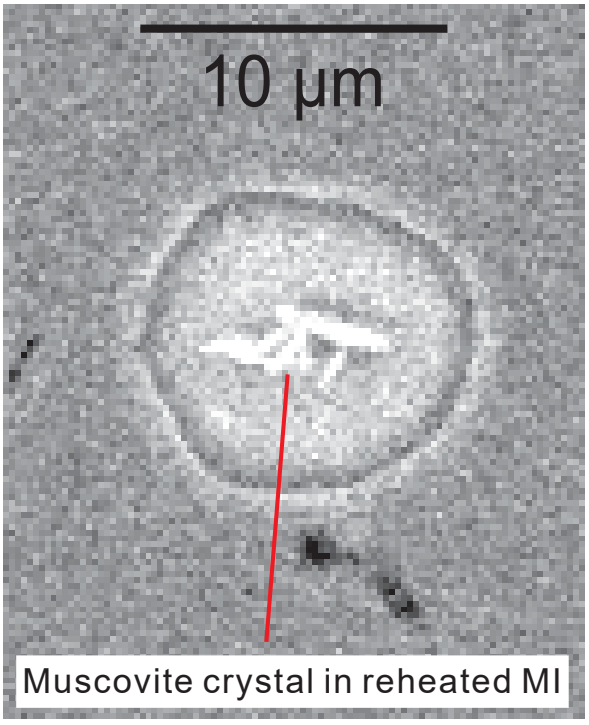

Figure OM4. MI containing muscovite crystals plus glass in a reheated melt inclusion from crystal A5. The MI is interpreted to have either trapped muscovite along with melt, or the muscovite formed after trapping as a result of reaction between K-feldspar and water released from the melt during cooling. Higher Al_2O_3 and TiO_2 contents determined during EDS analysis of the MI are interpreted to reflect mixed analyses of muscovite and silica-rich glass.

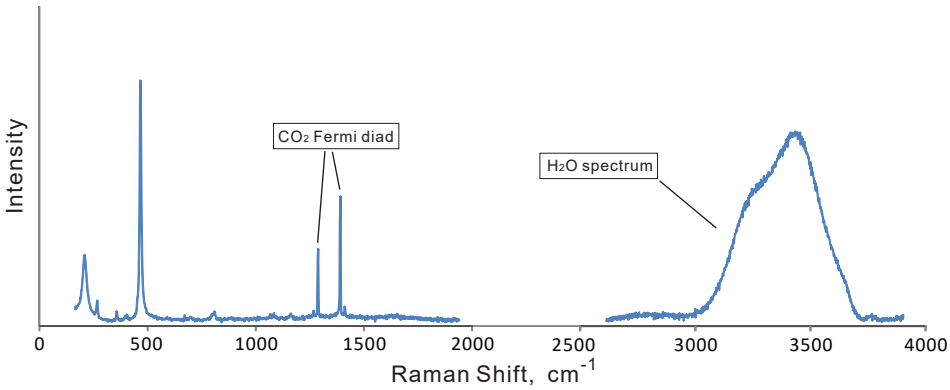

FIGURE OM5. Representative Raman spectrum of an H_2O-CO_2 fluid inclusion showing the Fermi diad for CO_2 and the broad band corresponding to liquid H_2O.

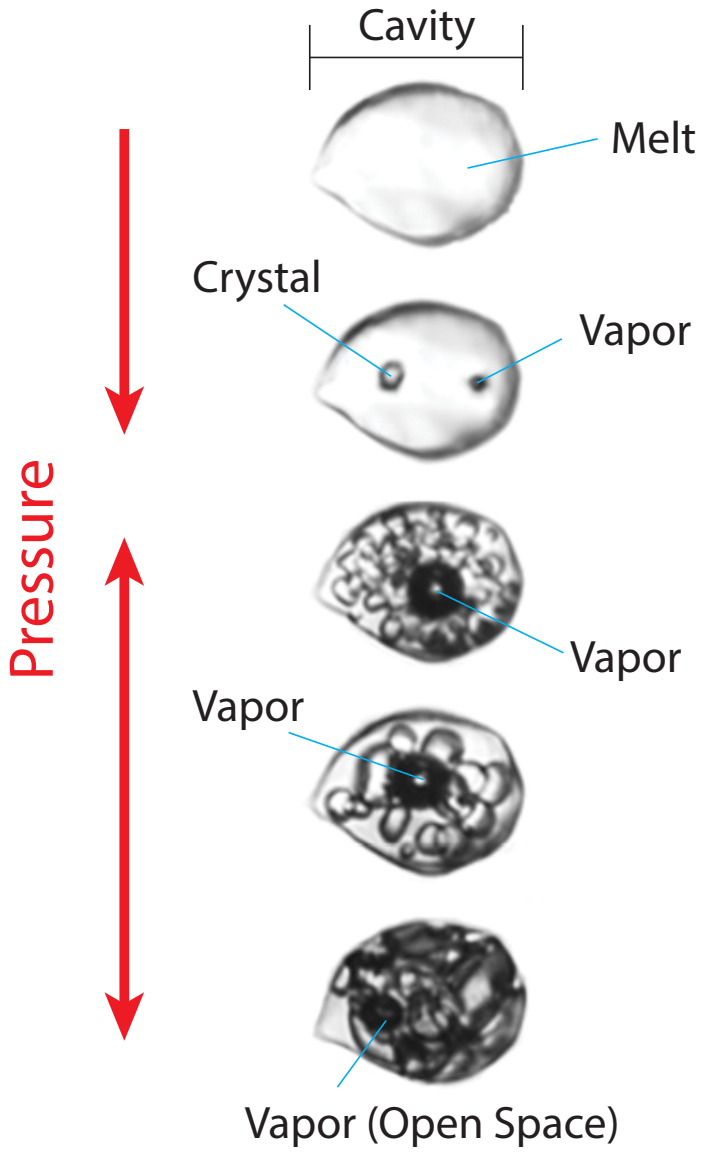

Figure OM6. Pictorial representation of the ripening or coarsening of crystals proposed for formation of the Taishanmiao pegmatites as illustrated by the phase behavior in a saline aqueous fluid inclusion during heating and cooling. The completely homogenized inclusion at the top (labeled "Melt") represents the residual melt that remains after crystallization of ~96% of the Taishanmiao granite at 734°C and 3.3 kbar. The second image from the top represents the pegmatite after some small amount of crystallization in a closed, isochoric system to produce a small crystal and a vapor bubble representing an H_2O-CO_2 fluid that has exsolved from the melt owing to the pressure decrease associated with crystallization. As the pegmatite body continues to slowly cool, the pressure fluctuates in a complex, nonlinear manner, leading to repeated episodes of crystal dissolution and precipitation that initially produce a mixture of fine-grained crystals (third image from top). Small crystals that dissolve during an episode of dissolution do not grow back during the next cycle of precipitation. Rather, the dissolved material precipitates onto existing larger crystals in the melt, leading to an overall ripening (coarsening) of the crystals with time as the system evolves (fourth and fifth images from the top), and this results in the pegmatitic texture that characterizes miarolitic class, segregation-type pegmatites containing large crystals and a void space.